DOI: 10.24352/UB.OVGU-2018-025 TECHNISCHE MECHANIK, 38, 2, (2018), 135 – 147
submitted: September 20, 2017

A Markov Chain Approach to Damage Evolution in Die-Cast ZAMAK

T. F. Korzeniowski, K. Weinberg

ZAMAK components typically have a high load-bearing capacity but show large variations in their limit loads and in the number of life cycles they can sustain. In this paper a new stochastic approach to account for accumulated damage is presented where weakening effects, such as impurities, pores and cracks, are considered as distributed defects and a Markov process is used to model the defect evolution. The basic ideas of this stochastic model are presented and sample calculations on die-cast ZAMAK components illustrate the field of application and the versatility of this approach.

1 Introduction

The failure of engineering constructions is strongly connected with reliability and life expectation of structural materials. As a consequence of loading, defects like pores, flaws and cracks evolve in the material, with their growth and finally coalescence being the basic failure mechanism in fracture, cf. Tvergaard (1990); Thomason (1990); Radaj and Vormwald (2007). Typically, the size of the defects is small compared to the size of the body and their distribution can only be determined by tomography scanning. The mechanisms of defect growth are diverse and hard to capture by material modeling; numerous attempts have been made and several deterministic models are developed, cf. Lemaitre and Chaboche (1998); Rösler et al. (2006); Kuna (2013) and references therein. Here we resort to a stochastic modeling and use a Markov process to describe the evolution of defects till failure. Markov processes have been applied to many different branches of science, e.g. in mathematical finance, actuarial science, queueing theory and mathematical biology (Bharucha-Reid, 1997). There are also attempts made to use them for the prediction of fracture mechanical problems, such as risk estimates (Cronvall and Männistö, 2009), crack propagation models (Gansted et al., 1994; Xi and Bazant, 1997), or fatigue crack propagation (Spencer Jr. and Tang, 1988; Lee and Park, 1998). We will employ this methodology here to study the failure of die-cast ZAMAK components.

ZAMAK (Zinc, Aluminum, Magnesium and Copper, german: Kupfer) alloys are frequently used in industry, their ability to be cast in small and fine components with high precision are attractive for many applications. The addition of aluminum ($\approx 4\%$) to zinc makes the alloy better manageable and improves the mechanical properties. Copper ($\approx 1\%$) is used for dissolution of aluminum in zinc and to increase the hardness. However, with increased copper content the ductility reduces and the material embrittles. To control inter-crystalline corrosion a small amount of magnesium is admixed. The lion's share of industrial application takes the ZAMAK alloy ZP 0410 which is composed of 3.8-4.2% Al, 0.7-1.1% Cu and 0.035-0.06% Mg (EN1774).

A common manufacturing process for ZAMAK is die-casting, which is characterized by forcing the molten alloy under high pressure into a mold cavity. The low melting temperature, together with relatively low costs, allow a highly productive process which is particularly well suited to the manufacturing of thin-walled components. These small parts show a high load-bearing capacity and are typically employed for heavy-duty components like hinges, pins, bearings and connections. Such window hardware is produced by the company Siegenia-Aubi KG which offers a wide range of components from hardware for windows and French windows to building technology for automation and intruder protection, many of them made of ZAMAK, see Fig. 1. Therefore the material's properties are of great interest and, based on a longer cooperation of our group with Siegenia-Aubi KG, the company supports this research by providing material specimen, experience and experimental data (Dinger, 2011).

Figure 1: Typical ZAMAK components for window hinges.

A typical die-casting process can be summarized in three main steps: preparation, casting and follow up. Before casting the alloy needs to be molten and the mold has to be prepared, e.g. with a lubricant. After opening of the machine, the melt is rapidly pressed into the mold and then pressurized for solidification. After solidification the casting needs to be reworked, e.g. scrap needs to be removed. The high pressure casting results in a fine micromorphology of the alloy. However, one downside of this casting process is a high air entrapment in the cast which leads to a high population of pores, see Fig. 2. From experience three phenomena are known in die-cast ZAMAK which result in a decay of its high strength and reliability (Dinger, 2011):

- reduction of strength in the course of time
- creep deformation
- dimensional change up to 1% as result of aging

All three phenomena are thermally activated processes and due to the low melting temperature, zinc alloys age even at room temperature.

From the industrial point of view volume changes can be marginalized by tempering and thus they will not be considered here. Also, we do not plan to explicitly study creep deformations. Under isothermal conditions creep is a long term process of plastic deformation which has its origin in morphological changes but is usually described phenomenologically. We will instead focus on aging in the sense of a decay of mechanical strength, induced by the pores and defects of the die-casted component. Such aging phenomena have been reported in Kallien and Leis (2011a), where different ZAMAK alloys have been studied and e.g., a dependence of the long term resistance from the components' wall thickness has been shown. However, to the authors knowledge there are no investigations on the interplay of micromorphology and mechanical properties of ZAMAK.

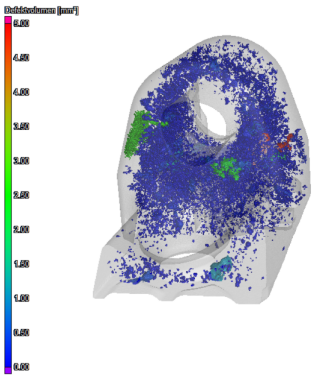

Figure 2: CT-scan of a part of a window bearing with pores of different size.

Here we circumvent the rare knowledge on ZAMAK by describing the evolution of defects, pores and cracks — which we will all summarize as voids subsequently — as a stochastic process. Note that in this work no geometry of the void is assumed. The remaining of this paper is organized as follows: In Section 2 we briefly introduce the basics of a Markov process. Section 3 provides a short overview of material fatigue and introduces a damage parameter. In Section 4 numerical examples are presented, we start with a parametric study to show the basic behavior of the model and go on with a life-estimation for a ZAMAK window hinge. In section 5 the paper is concluded.

2 The Markov Process

In order to describe the evolution of the void distribution by a Markov chain we begin with the basic definition of a Markov process (Kulkarni, 2016).

A stochastic process $(X_t, t \in \mathbb{N})$ on an at most countable state space $Z = \{z_1, z_2, \dots\}$ is called a discrete

Markov process or Markov chain, (Markov, 1906), if the following holds for every $z \in Z$:

$$P(X_{t+1} = z_{t+1}|X_t = z_t, X_{t-1} = z_{t-1}, \ldots, X_0 = z_0) = P(X_{t+1} = z_{t+1}|X_t = z_t)\,. \tag{1}$$

Equation (1) states that one can make predictions for the future of the process based solely on its current state. The transition probabilities depends only on the state X_t and not on the past states $X_0, X_1, \ldots, X_{t-1}$, a property which is often referred to as the Markov property. The process is described by a transition matrix $\boldsymbol{P}$ with the transition probabilities $p_{i,j} = P(X_{t+1} = z_j|X_t = z_i)$ to move from state i to state j

$$\boldsymbol{P} = \begin{pmatrix} p_{1,1} & p_{1,2} & \cdots & p_{1,j} & \cdots \\ p_{2,1} & p_{2,2} & \cdots & p_{2,j} & \cdots \\ \vdots & \vdots & \ddots & \vdots & \ddots \\ p_{i,1} & p_{i,2} & \cdots & p_{i,j} & \cdots \\ \vdots & \vdots & \ddots & \vdots & \ddots \end{pmatrix}. \tag{2}$$

This matrix, together with the starting distribution, determines the stochastic behavior of the Markov chain. The transition matrix can be used to compute the state of the chain at any desired time step via

$$z_t = z_0 \boldsymbol{P}^t \tag{3}$$

where z_0 is the initial state and z_t, respectively, the state at current time t. Furthermore, we introduce absorbing states if the probability to leave this state is zero, i.e. $p_{i,i} = 1$ and $p_{i,j} = 0$, $i \neq j$.

To model the microstructural evolution in ZAMAK we assume the defects to grow with a certain probability in every cycle of loading. The idea is to describe the transition of the defect distribution from a time t to the next time $t+1$ by means of the Markov chain as illustrated in Fig. 3. We use a time-homogeneous Markov chain on a finite state space

$$S = \mathcal{S} \cup \mathcal{A} = \{s_1, s_2, \ldots, s_M\} \cup \{a_1, a_2, ..., a_M\} \tag{4}$$

with $\mathcal{S}$, the set of growing states, and $\mathcal{A}$, the set of absorbing states. The states ought to be characterized by a size describing parameter, e.g. a micro-crack length, spall plane or void volume. Specifically we use here a characteristic void size (length).

The absorbing states of the Markov process may have different reasons. It is possible that some defects cannot grow because of local obstacles and are therefore trapped in an absorbing state. Some other defects or voids may coalesce and then one void may jump into an absorbing state. For example, we take a look at a void which starts in the state $m = s_1$ in the given transition graph in Fig. 3. Then there is the chance p_1 to grow a specified amount, which is state $m = s_2$, a chance $\tilde{p}_1$ to stay in current state $m = s_1$, or a chance of $1 - p_1 - \tilde{p}_1$ to reach the absorbing state a_1. Being in the state $m = s_2$ it has again the probability p_2 to grow, $\tilde{p}_2$ to stay in state $m = s_2$ or it reaches with probability $1 - p_2 - \tilde{p}_2$ the absorbing state a_2. This is again repeated until the void reaches an absorbing state, see Fig. 3 for an illustration. The state s_M is the maximum possible size a void can reach.

3 Metal Fatigue

Material fatigue describes progressive weakening of a material caused by repeatedly applied loads. From the mechanical point of view the problem is to estimate the defect growth after N steps of cyclic loading.

3.1 Fatigue-life Prediction and Defect Distributions

If the component is heavily loaded and some plastic deformations occur it typically withstands only a low number of cycles. If the overall stresses are low and the deformation is primarily elastic, the material weakens by high-cycle fatigue, i.e. failure only occurs after more than 10^4 cycles. The nominal maximum stress values are here much smaller than the strength of the material.

For engineering applications it is of high importance to know the limit of load cycles a component can sustain before failure. The experimental way to describe fatigue is the Wöhler experiment which

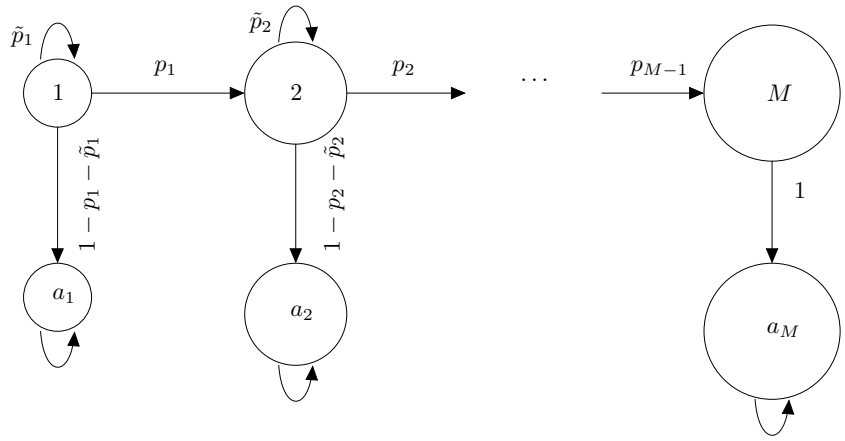

Figure 3: Markov-chain with transition rates to model growth. It is possible to built in movements on the horizontal line where states get bypassed.

is normed, e.g. in DIN 50100. Several copies of the same component are subjected to a sinusoidal stress. After failure of those copies the number of cycles are plotted against the applied stress, often on a logarithmic scale. The arising curve is named Wöhler curve or S-N curve. The issue with such experiments is that even for the same component and the same loading, the results will not be the same due to microstructural differences and geometric effects. One could do a higher number of experiments for the same stress to describe the resulting number of cycles by a probability distribution. Typical distributions used in describing fatigue are the log-normal, extreme value, Birnbaum-Saunders and the Weibull distribution (Bhattacharyya and Fries, 1982; Weibull et al., 1949). Whereas the latter is ultimately connected to failure, the first distributions may also describe probabilistic influences.

As the ultimate tensile stress limit is completely in the elastic range of the material, a classical dimensioning or a finite element analysis of such situations does not lead to any prognosis. Therefore the actual life expectation of high-cycle loaded structures is often only roughly estimated by using, e.g., Paris' law for fatigue crack growth (Rösler et al., 2006; Radaj and Vormwald, 2007). Other approaches to fatigue-life prediction assume micro-crack growth and use a cohesive loading envelope, (Serebrinsky and Ortiz, 2005; De Moura and Gonçalves, 2014). However, the consideration of each stochastic feature, multiaxial loading or non-linear material behavior requires a certain amount of tweaking and additional adjusting which calls into question the predictive ability of the fatigue model.

Therefore, we propose here a stochastic approach where we summarize all weakening effects, such as precipitating impurities, nucleation and growth of pores as well as micro-cracks under the term *void*. We assume an initial distribution for the voids, which will be based on the distribution of pores determined initially before testing. These distributions are often assumed log-normal, cf. (Brakel, 1975), as this is the natural limit arising in the central limit theorem for products. Other positive, right-skewed distributions could also be employed, cf. Reppel et al., and regarding the limited solution of computed tomography (CT) scans, an exponential distribution starting with the first identifiable pore size can be a sufficient approximation. The evolution of the population of voids is then modeled by a Markov chain which provides an simple way to estimate the number of life cycles.

3.2 Model Parameter and Experimental Data

The key for the success of the model is experimental data. Some parameters need to be determined from the initial microstructure, ideally by CT scans. An initial void size distribution can be deduced out of an image analysis. Additionally, a maximum size of the void needs to be set as input parameter for every Markov chain. It defines the final absorbing state a_M and can also be determined from micrographs. Please note that here and in the following we define the state of the defect by its normalized void size, i.e.,

$$s_i(\boldsymbol{x}, t) = \frac{r_i(\boldsymbol{x}, t)}{r_{\text{ref}}}\,, \tag{5}$$

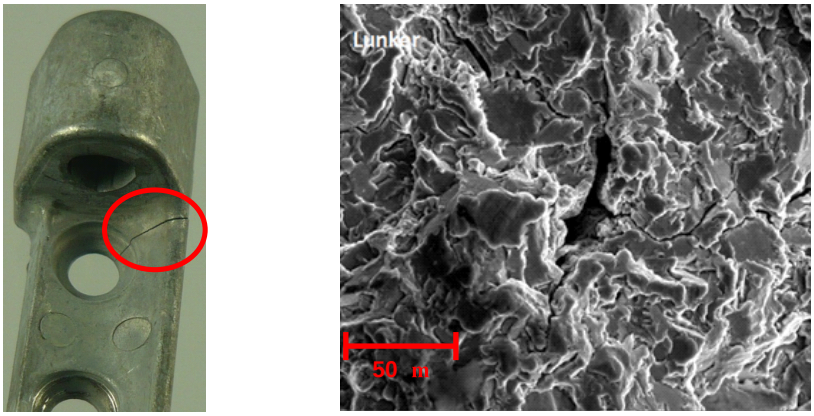

Figure 4: Position of the crack in cyclic loading of the tilt window experiment (left) and REM micrograph of the failure surface with a crack initiated from a cavity in the middle (right); photographs from Dong (2017).

with the reference size to be given by the specific problem. Here we set $r_{\text{ref}} = 1\mu\text{m}$. The states as well as the typical void size $r(\boldsymbol{x}, t)$ depend on the local position $\boldsymbol{x}$ within the investigated domain, whereby $\boldsymbol{x}$ defines the position of a material point, i.e., a unit volume of the component.

In order to obtain the experimental data, high cycle experiments simulating the sudden opening of a window were performed. The applied load corresponds to the impact of window opening in tilt position and was repeatedly applied till failure of the hinges, cf. Dong (2017). In Fig. 4 the typical failure is shown and in the micrograph it can be seen that the failure was typically initiated from cavity induced cracks. In this sense we define here a 'failure parameter' for crack growth, i.e. a critical defect volume fraction. To this end we presume the initial defect volume per unit volume $D_0(x) = D(t = 0, x)$ to be small and determined by $D_0(x) = \sum_{i=1}^{2M} \#s_i(0, x) \cdot r(s_i)$, where $\#s_i(0, x)$ is the number of voids in state s_i at the initial timepoint and position $\boldsymbol{x}$ and $r(s_i)$ is the size described by state s_i. For engineering metals, the specific initial defect volume is in the range of $D_0 = 10^{-4} \dots 10^{-2}$, Tvergaard (1990). This value corresponds to the defect volume measured in the initial CT scans of our window hinges, $D_0 = 1.4\%$.

The growth of defects will ultimately lead to component failure. The material is expected to be intact as long as the size of the defects in the observed location

$$D(\boldsymbol{x}, t) = \sum_{i=1}^{2M} \#s_i(\boldsymbol{x}, t) \cdot r(s_i) \tag{6}$$

is below a critical size

$$D_t \leq D_{\text{crit}}. \tag{7}$$

In the course of their life the component experiences a number of loading cycles N. The variable of interest is the number of cycles when the component fails, N_c.

To deduce N_c from the model, we need a parameter that determines when the regarded component shall be considered as broken. If a pore analysis is available from CT scans of broken components, a 'failure distribution' at the point of interest can be concluded. It is then possible to compare the volume of the failure distribution to the pore size distribution in the actual simulation. Other, more simple examples for a failure parameter can be the mean of the given distribution, the median, the biggest pore size or, as used in this paper, the total defect volume.

The unknowns, which still remain to be determined, are the transition probabilities p_i that determine the behavior of the Markov chain. These probabilities could be related to a material model, however, this would jeopardize the simplicity of the stochastic approach. Instead we suggest to relate the probabilities directly to the main loading parameters at the position of interest, i.e.,

$$p_i = p_i\left(s_i, R_m, \sigma_{\max}\right) \qquad i = 1, \dots, M\,. \tag{8}$$

where s_i is the i-th state (5), R_m is the material resistance and $\sigma_{\max}$ is the maximum principal stress at the position of interest. Other dependencies may, of course, be added.

4 Numerical Examples

In this section the evolution of damage in a typical die-cast component will be tracked exemplarily. To this end we will at first use a dimensionless toy problem to illustrate the properties of the chosen stochastic method. Subsequently follows the application of the Markov chain approach for life-estimation of a window hinge.

We begin by stating the state space (4). Because we describe the material's defects by a size describing parameter, the real interval $[0, r_{\max}]$, will be divided into an arbitrary number of M intervals $[r_i, r_{i+1}], i = 0, ..., M-1$. For these intervals it holds

$$\bigcup_{i=0}^{M-1} (r_i, r_{i+1}] = (0, r_{\max}] \qquad \text{and} \qquad (r_i, r_{i+1}] \bigcap (r_j, r_{j+1}] = \emptyset, i \neq j \tag{9}$$

with $r_0 = 0$ and $r_M = r_{\max}$. Given the same transition graph as displayed in Fig. 3, the corresponding transition matrix has the form:

$$\boldsymbol{P} = \begin{bmatrix}
\tilde{p}_1 & p_1 & 0 & 0 & \dots & 0 & 1-p_1-\tilde{p}_1 & 0 & 0 & \dots & 0 \\
0 & \tilde{p}_2 & p_2 & 0 & \dots & 0 & 0 & 1-p_2-\tilde{p}_2 & 0 & \dots & 0 \\
0 & 0 & \tilde{p}_3 & p_3 & \dots & 0 & 0 & 0 & 1-p_3-\tilde{p}_3 & \dots & 0 \\
\vdots & \vdots & \vdots & \ddots & \ddots & 0 & \vdots & \vdots & \ddots & \ddots & 0 \\
0 & 0 & 0 & 0 & \ddots & p_{M-1} & 0 & 0 & 0 & \ddots & 0 \\
0 & 0 & 0 & 0 & \dots & \tilde{p}_M & 0 & 0 & 0 & \dots & 1 \\
0 & 0 & 0 & 0 & \dots & 0 & 1 & 0 & 0 & \dots & 0 \\
0 & 0 & 0 & 0 & \dots & 0 & 0 & 1 & 0 & \dots & 0 \\
0 & 0 & 0 & 0 & \dots & 0 & 0 & 0 & 1 & \dots & 0 \\
\vdots & \vdots & \vdots & \vdots & \ddots & \dots & \vdots & \vdots & \vdots & \ddots & \vdots \\
0 & 0 & 0 & 0 & \dots & 0 & 0 & 0 & 0 & \dots & 1
\end{bmatrix}.$$

Please note that there is always the chance to change the transition graph of the Markov-process like desired, e.g. to built in transitions we do not consider here.

4.1 Parametric Study

We start with a simple state space of $M = 25$ states with $r_{\max} = 10\,\mu$m and chose a uniform and constant transition probability $p_i = p_j$ for every state $i = 1 \dots M$ and $j = 1 \dots M$. Furthermore we set $p_i + \tilde{p}_i = 1$ at first, so that there are no absorbing states. These leads to the same transition matrix as in Lee and Park (1998) and Xi and Bazant (1997).

Results of the first calculations can be seen in Fig. 5. Each row stands for a different simulation where the initial distribution was varied. 10000 random numbers were generated with a given initial distribution and then classified into $M = 25$ states. These initial distributions are shown in the left column of Fig. 5. In the middle column of Fig. 5 the corresponding states after 1000 steps of the Markov process are displayed. Because the voids of all states are growing we see that the distribution moves to the right. Also, we see that the shape changes towards a normal distribution. The described phenomena continues in graphs of the right column of Fig. 5, where the states are shown after 5000 processes. The more steps are used the more the initial distributions of the states changes to the shape of a normal distribution, but a student distribution provides a better fit for the first four initial distributions, i.e., there will be a mean void size with a certain deviation. This is a consequence of the structure of the transition matrix with constant entities p_i. In the last row a normal distribution fits better.

At next, we vary the transition probability which now has to depend on the current state. To this end we assume a function $g : \mathcal{S} \to [0, 1]$, $g(s_i) = p_i$, which gives the transition probabilities for a given state. We use an increasing third order polynomial g_1, a decreasing g_2 as well as a parabola g_3 with minimum at 25 for this function. The functions read as follow $g_1(s_i) = 5.1852 \cdot 10^{-6} s_i^3 - 1.1667 \cdot 10^{-4} s_i^2 + 0.01$, $g_2(s_i) = -4.0000 \cdot 10^{-6} s_i^3 + 9 \cdot 10^{-5} s_i^2 + 0.0022$ and $g_3(s_i) = 2 \cdot 10^{-4} s_i^2 - 0.0030 s_i + 0.015$. The functions as well

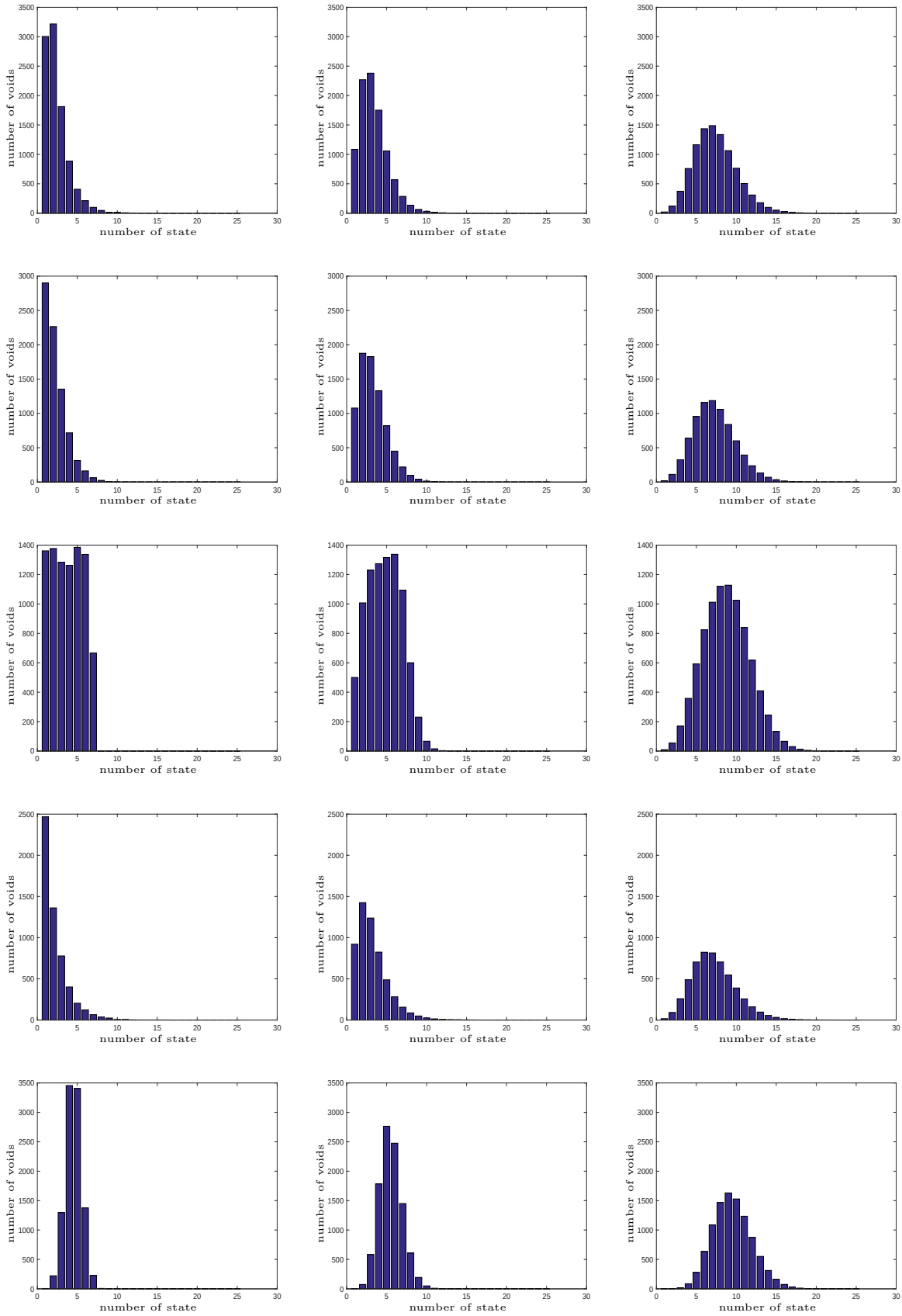

Figure 5: Evolution of the size distribution in a Markov process with constant entities p_i. Every row is a new simulation with a different initial distribution. The initial distribution are in the following order: log-normal, weibull, uniform, exponential and normal distribution. The following columns are after 1000 and 5000 applications.

as the initial distributions are displayed in Fig. 6. We displayed the continuous versions of g for better visibility, although we are only interested in the discrete values $g(s_i)$. To better see the evolution of the distribution, the number of states is now increased to 50. The functions are displayed in the right picture of the first row. The initial distribution is displayed on the left side, and in the second row the distribution in states is given after 1000 steps. In (c) the decreasing polynomial is used, in (d) the increasing polynomial is used, and in (e) the parabola is used. Note that $g(50)$ is zero as there exists no state above. The initial distribution was a log-normal distribution with parameters $\mu = 0$ and $\sigma = 0.6$. In (c) the higher probabilities at the lower states lead to a big change in the left tail which becomes very smooth. The long right tail of the initial distribution disappears in consequence of the low probabilities at the high states. In contrast, in (d) the higher probabilities at the high states lead to a long right tail while the left tail does not change significantly. The parabola in the last row combines both, the higher probabilities at the low states in difference to those state in the middle leads to a short left tail. The low probabilities in the middle states lead to a very low amount of voids in the right tail but the higher probabilities at the higher states lead to a long right tail, which can hardly be seen in the picture.

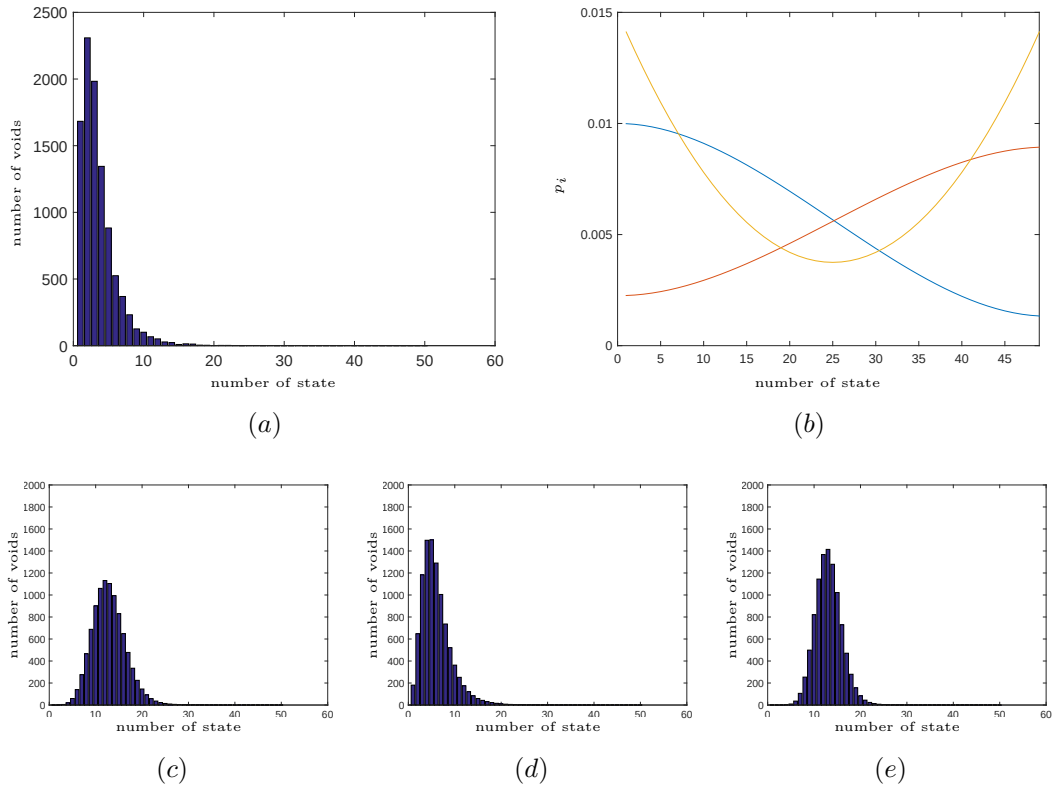

Figure 6: Studies for different jump functions: In (a) the initial distribution of states is displayed. The three functions in (b) are the probabilities to jump into a the next higher state, $p_i = g(s_i)$. In the lower row the results are displayed after 1000 steps for (c) a decreasing function $g(s_i)$, (d) an increasing function $g(s_i)$, and (e) the parabola function $g(s_i)$.

Such a dependence of the transition probability on the state may be physically motivated. For example, in static fracture experiments with ductile specimen we usually observe a cup-cone-like fracture with plastic straining and a very dimpled fracture surface with small and big voids. This corresponds to initially distributed micro-voids which all grow with similar probability. In consequence, this leads to a Student's distribution (a distribution that differs from a Gaussian by having power law tails) like in Fig. 5, cf. Ponson et al. (2013). In dynamic ductile fracture the effect of void growth is different, cf. Weinberg et al. (2006). Here the final void distribution shows a smaller variety of void sizes, i.e., the smaller voids seem to grow faster than the bigger ones. Therefore the evolution of the distribution function which evolved in Fig. 6c is very much alike the one in Weinberg and Böhme (2008), where a specific constitutive law was derived from the micromechanical mechanisms of void growth in a viscoplastic solid.

From material science it is well known that, on the one hand, pores grow only at a critical cavitation size, cf. Weinberg and Böhme (2009), and, on the other hand, large pores grow at the expense of the

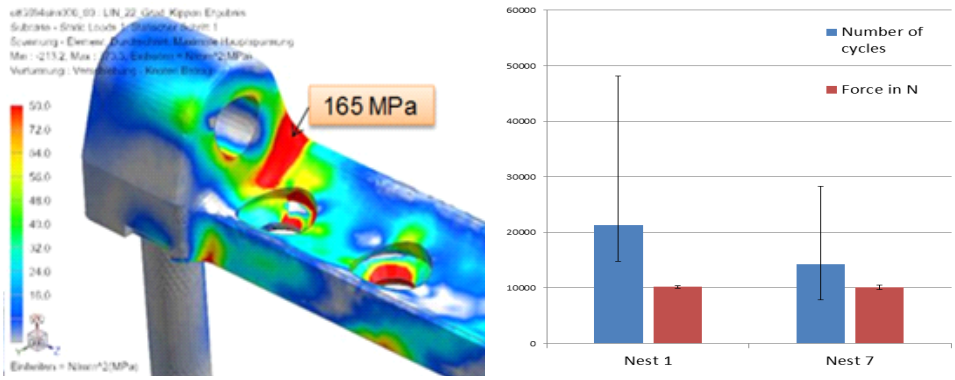

Figure 7: Maximum principal stress values computed in a finite element analysis (left) and experimental results of cyclic loading until failure for a set of 29 specimen which had been die cast in nest 1 of the mold and another set of 25 specimen which had been cast in nest 7 (right); displayed are also the maximal forces measured in a rupture test.

smaller ones. The first effect of a critical nucleation size can be captured by a low transition probability for small states, Fig. 6d, whereas the second effect, which is known as Oswald ripening, can be modeled by a decreasing 'jump function'.

4.2 A Markov Chain Approach for Life-Estimation

Here we will apply our Markov chain approach for the life-estimation of a ZAMAK window hinge. We consider the die-cast component of the hinge as displayed on the right hand side of Fig. 4. The initial porosity has been determined for several of these parts by CT scans, see Fig. 2. Additionally, several experimental investigations on the endurance in cyclic dynamic loading have been performed with the aim to find material or design dependent factors of influence, cf. Dong (2017). These experimental results will serve us here as a data basis for our modeling.

Please note that we simulate here the growth of defects in the whole die-cast component, i.e., our approach is macroscopic. Generally, it is also possible to use the Markov chain model within a finite element analysis, i.e., like a constitutive law at every integration point. Then the transition probabilities depend additionally on the position $\boldsymbol{x}$. This, however, would require a deeper knowledge on the functional dependence of the probabilities which is beyond the scope of this paper.

In order to determine the load dependence we refer to the experiments. They have been performed for the situation of dynamic window opening, i.e., the initial load is close to zero and at impact the stress reaches a maximum. Fig. 7(left) shows the maximum principal stress $\sigma_{\max}$ obtained from a finite element analysis of the tilt window position. A static analysis has been performed with loading assumption which correspond to the maximal impact forces measured in abrupt opening experiments. The position of the maximum stress, $\sigma_{\max} = 165\,\mathrm{MPa}$, corresponds to the location of failure. In consequence we later define a load dependent factor Θ to determine jump probabilities.

The set $\mathcal{S}$ will be the real interval $[1, 15]$ divided into $M = 100$ states. The state space S is completed with 100 absorbing states, i.e.,

$$S = \mathcal{S} \cup \mathcal{A} = \{s_1, s_2, \ldots, s_{100}\} \cup \{a\}_{i=1,100} \tag{10}$$

with $r_i - r_{i-1} = 0.14$ according to equation (9).

For the ZAMAK component we model the jump probabilities as a function of the form (8). Specifically we make use of an increasing third order polynomial approach like in Fig. 6 so that the function is able to generate higher jump rates in the higher states. In this sense we model the transition probability $p_i = g(s_i)$. We set

$$g(s_1) = \Theta/4,\ g(s_{M-1}) = \Theta,\ g'(s_1) = g'(s_{M-1}) = 0$$

to determine the function $g(s_i)$. Using

$$\Theta = \frac{\sigma_{\max}^2}{R_m^2 M} = 2.101 \cdot 10^{-3}$$

where we assume a material resistance of $R_m = 360\,\mathrm{MPa}$, cf. Kallien and Leis (2011b), leads to the following jump probabilities

$$p_i = -9.34 \cdot 10^{-7} s_i^3 + 2.10 \cdot 10^{-5} s_i^2 + 5.25 \cdot 10^{-4}. \tag{11}$$

Remember that the final state has always a jump probability of zero. We also introduce absorbing states which account, e.g., for obstacles in crack propagation or coalescence of voids. With

$$1 - p_i - \tilde{p}_i = a_i,$$

we set $a_i = 6 \cdot 10^{-6}$ for every state i. The prior formula also gives the resulting values of $\tilde{p}_i$ which are the probabilities to stay in the current state.

The initial voids typically have a logarithmic distribution. In the die-cast hinge components we observe initial void distributions which depend on the position during casting. Within the die-cast process, seven components form a so-called nest of molds and are cast simultaneously. In particular, one position was identified to lead to a number of large voids whereas the overall porosity is almost equal in all positions. Therefore we consider two different initial log-normal distributions: for the simulations of nest 1 the initial parameters were $(\mu, \sigma) = (-0.2133, 0.4)$ and for the simulations of nest 7 the parameters were $(0.1971, 0.4)$, see Fig. 8. As failure parameter a final overall porosity of 4% was chosen, so the simulation runs as long as

$$D(\boldsymbol{x}, t) = \sum_{i=1}^{2M} \#s_i(\boldsymbol{x}, t) \cdot r(s_i) \leq 0.04 \tag{12}$$

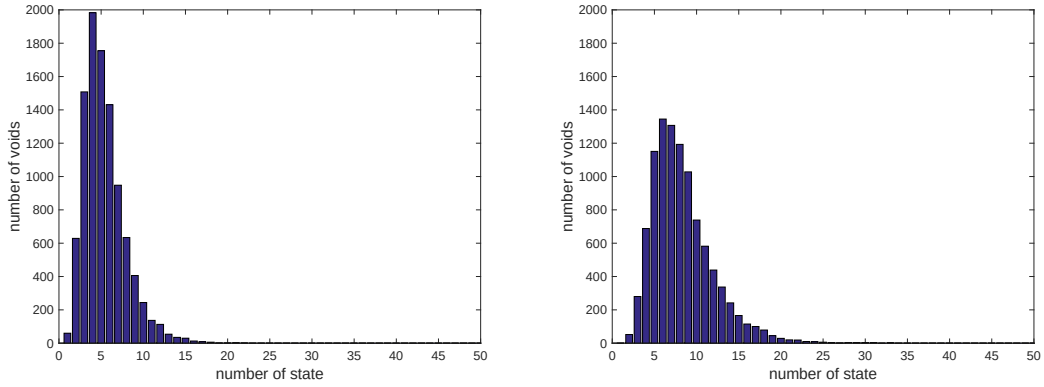

Figure 8: The two initial distributions of voids for nest 1 (left) and nest 7 (right).

With both initial distributions we calculated the evolution of defects until the failure parameter is exceeded. Each Markov step corresponds to one load cycle. The distribution which exceeds the damage parameter at first is the one of nest 7 (Fig. 8, right). The experimentally determined life expectation is plotted for both sets of specimen in Fig. 7. Experimental results of cyclic loading for a set of 29 specimen which had been die-cast in position Nest 1 of the mold and another set of 25 specimen which had been cast in position Nest 2 are shown. All specimen fail in the same position of the part, as indicated in the photograph of Fig. 4. The mean values of the experimentally determined number of life cycles are 21752 for nest 1 and 14231 for nest 7. In the right of Fig. 7 also the maximal forces measured in a rupture test are plotted. Here we do not see any influence of the void distribution, only the overall porosity determines the maximum load at failure.

In Fig. 9 the computational results of the window hinge example are shown. In the first row the function $g(s_i)$ is displayed which shows the probabilities to jump into a higher state (a). In (b) a state distribution

is displayed which just exceeded the failure parameter. The absorbing states can also be seen here. In the second row the distribution of lifetimes is shown for simulations of nest 1 (right) and nest 7 (left). Like expected the simulations of nest 7 stop earlier because the initial distribution contains bigger voids. The number of cycles in the simulations of nest 1 and 7 are 27138 and 20217, respectively. The tendency is the same like in the experimental investigation but both numerical values are about 20% higher. A better quantitative agreement of experiments and calculations would require a more sophisticated modeling of the transition probabilities and is subject of ongoing research. Additionally, a stochastic noise could be added to the initial distribution parameters in order to replicate the scattering of the results. Such a noise would correspond to the large variation of results observed experimentally in both nests.

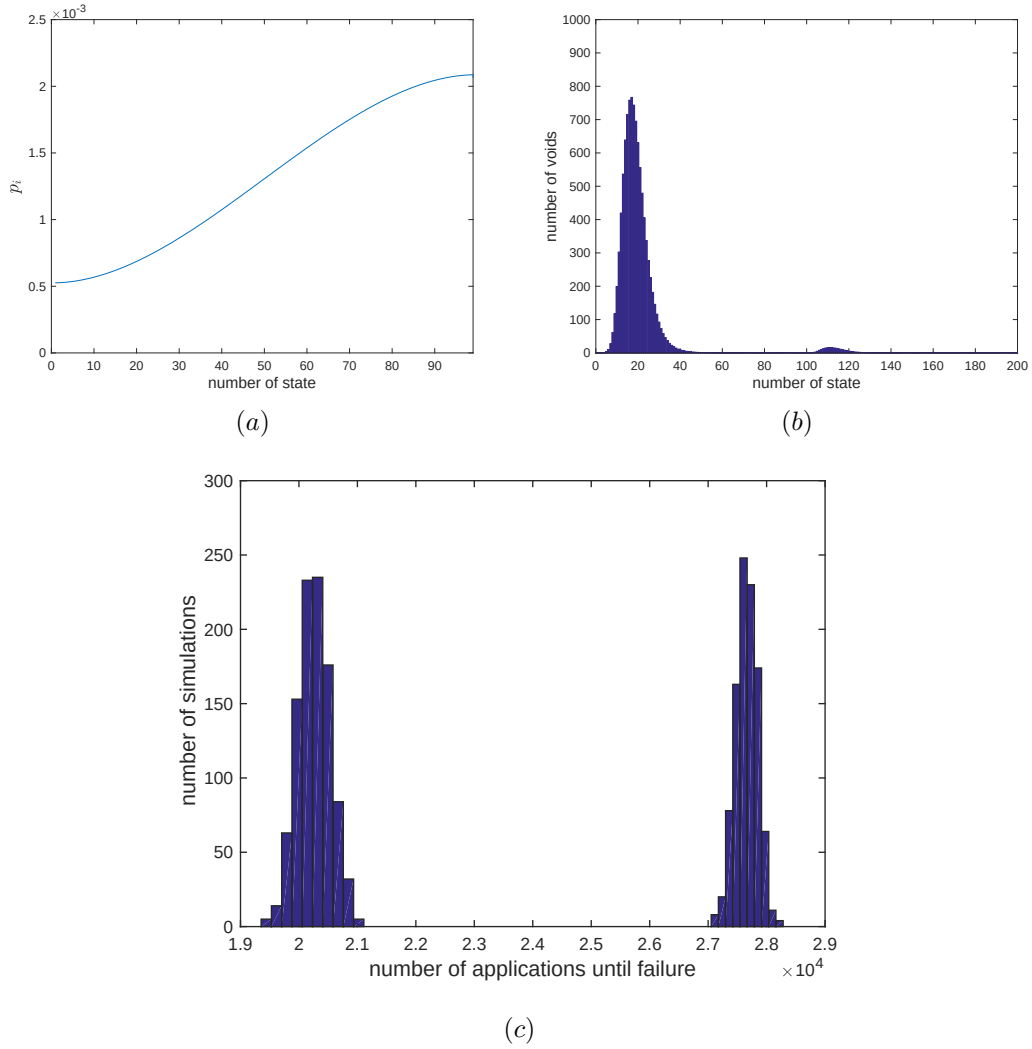

(a) (b) (c)

Figure 9: Simulation of life cycles: On the left side in the upper row the jump function $g(s_i)$ is displayed. On the right side a distribution of voids is displayed where the simulation stopped as the failure parameter is exceeded. In (c) the distribution of the lifetimes is displayed for the simulations of nest 1 (right) and nest 7 (left).

We conclude that with a physical motivated and neat selection of the parameters we are able to obtain results which are in accordance with the experiments. A predictive computation, however, requires a profound modeling of the transition probabilities as a function of the material.

5 Conclusion

Summarizing, we state that ZAMAK is — from the material science point of view — well investigated. Various publications provide information on the characteristics of the (ideal) material. Nevertheless there is hardly any knowledge about its long term behavior, about its mechanical response under different loading conditions, and about the reasons of the large variations in its limit loads. This information,

however, is essential for predicting the mechanical behavior of die-cast ZAMAK components. Because a deterministic material model will have to account for a variety of physical phenomena and influences and will likely not be able to explain the scattering of failure parameter, we suggest here a stochastic modeling.

In our model the weakening influence of defects in a die-cast component subjected to cyclic loading is described by a Markov process. With this stochastic approach it is possible to estimate the evolution of damage for a given initial distribution. In simple examples we show the general effects of the initial state space, the number of process steps and the jump function on the final void distribution. A failure parameter determines the critical number of cycles, i.e., it indicates the defect distribution which will ultimately lead to component failure. The character of the Markov process is predominantly determined by the states' transition probabilities. The required stochastic parameter could be deduced from experimental results, especially from CT scans of the virgin component and the corresponding distribution at failure. Combined with an elastic finite element analysis, which provides the maximum elastic stress in the component, a jump function for the transition probability in critical zone of a widow hinge component can be found.

With the derived jump function we evaluated the defect growth in two sets of die-cast ZAMAK specimen. Because the die-cast process works with a concurrent cast of 7 parts, the location of these parts in the mold has an influence on the typical distribution of pores and voids. Experiments show that, although the overall porosity is similar, their number of cycles till failure differs. This could be captured by our Markov model with the computational result in agreement to the experimentally obtained data. Please note, that the failure load of a rupture test under monotone loading does not show such scattering.

In the future, our research on Markov processes shall focus on developing a more elaborate model for the transition probabilities. CT scan data will be used to generalize the construction of the jump function based on the specific cast material, the loading amplitude and on information about the defect distribution in the initial and in the failed state. This will enable us to predict the number of life cycles a component can sustain and it will support service life analyses of die-cast ZAMAK components.

Acknowledgement

We gratefully acknowledge the support of the Deutsche Forschungsgemeinschaft (DFG) under the project "A stochastic approach to damage evolution in die-cast zinc alloys" as part of the Priority Programme SPP1886 "Polymorphic uncertainty modelling for the numerical design of structures". We also thank the Siegenia-Aubi KG for providing experimental data.

References

Bharucha-Reid, A. T.: *Elements of the Theory of Markov Processes and Their Applications*. Dover books on mathematics, McGraw-Hill series in probability and statistics, Courier Corporation (1997).

Bhattacharyya, G.; Fries, A.: Fatigue failure models: Birnbaum-saunders vs. inverse gaussian. *IEEE Transactions on Reliability*, 31, 5, (1982), 439–441.

Brakel, J. V.: Pore space models for transport phenomena in porous media review and evaluation with special emphasis on capillary liquid transport. *Powder Technology*, 11, 3, (1975), 205–236.

Cronvall, O.; Männistö, I.: Combining discrete-time markov processes and probabilistic fracture mechanics in ri-isi risk estimates. *International Journal of Pressure Vessels and Piping*, 86, 11, (2009), 732 – 737.

De Moura, M.; Gonçalves, J.: Cohesive zone model for high-cycle fatigue of adhesively bonded joints under mode i loading. *International Journal of Solids and Structures*, 51, 5, (2014), 1123–1131.

Dinger, G.: Zusammenstellung von experimentellen Untersuchungen zu Alterungsvorgängen bei Zinkdruckgusslegierungen. Interner Bericht, Siegenia Aubi KG (2011).

Dong, Y.: Experimentelle Untersuchung von Einflüssen auf die zyklische Festigkeit von Zinkdruckguss Bauteilen. Master thesis, University Siegen (2017).

Gansted, L.; Brincker, R.; Hansen, L. P.: The fracture mechanical markov chain fatigue model compared with empirical data. Fracture and Dynamics No. 54, Dept. of Building and Structural Engineering, Aalborg University (1994).

Kallien, L. H.; Leis, W.: Ageing of zink alloys. *International Foundry Research*, 64, 2, (2011a), 23–27.

Kallien, L. H.; Leis, W.: Ageing of zink alloys. *International Foundry Research*, 64, 2, (2011b), 23–27.

Kulkarni, V. G.: *Modeling and analysis of stochastic systems*. CRC Press (2016).

Kuna, M.: *Finite Elements in Fracture Mechanics. Theory - Numerics - Applications*. Springer–Verlag, Berlin (2013).

Lee, O. S.; Park, C.: Fatigue life prediction by statistical approach under constant amplitude loading. *KSME International Journal*, 12, 1, (1998), 67–72.

Lemaitre, J.; Chaboche, J.-L.: *Mechanics of solid materials*. Cambridge University Press (1998).

Markov, A. A.: Extension of the law of large numbers to dependent quantities [in Russian]. *Izvestiia Fiz.-Matem. Obsch. Kazan Univ., 2nd Ser.*, 15, (1906), 135–156.

Ponson, L.; Cao, Y.; Bouchaud, E.; Tvergaard, V.; Needleman, A.: Statistics of ductile fracture surfaces: the effect of material parameters. *International Journal of Fracture*, 184, 1-2, (2013), 137–149.

Radaj, D.; Vormwald, M.: *Ermüdungsfestigkeit*. Springer (2007).

Reppel, T.; Korzeniowski, T.; Weinberg, K.: Stereological transition of right-tailed distributions - an overview with an application to polyurea. *to appear*.

Rösler, J.; Harders, H.; Bäker, M.: *Mechanisches Verhalten der Werkstoffe*. Teubner (2006).

Serebrinsky, S.; Ortiz, M.: A hysteretic cohesive-law model of fatigue-crack nucleation. *Scripta Materialia*, 53, 10, (2005), 1193–1196.

Spencer Jr., B.; Tang, J.: Markov process model for fatigue crack growth. *Journal of engineering mechanics*, 114, 12, (1988), 2134–2157.

Thomason, P.: *Ductile Fracture of Metals*. Pergamon Press (1990).

Tvergaard, V.: Material failure by void growth to coalescence. *Advances in Applied Mechanics*, 27, (1990), 83–151.

Weibull, W.; Weibull, W.; Physicist, S.; Weibull, W.; Physicien, S.; Weibull, W.: *A statistical representation of fatigue failures in solids*. Elander (1949).

Weinberg, K.; Böhme, T.: Mesoscopic Modeling for Continua with Pores: Dynamic Void Growth in Visco-Plastic Metals. *Journal of Non-Equilibrium Thermodynamics*, 33, 1, (2008), 25–49.

Weinberg, K.; Böhme, T.: Condensation and Growth of Kirkendall Voids in Intermetallic Compounds: Components and Packaging Technologies, IEEE Transactions on. *IEEE Transactions on Components and Packaging Technologies*, 32, 3, (2009), 684–692.

Weinberg, K.; Mota, A.; Ortiz, M.: A variational constitutive model for porous metal plasticity. *Computational Mechanics*, 37, 2, (2006), 142 – 152.

Xi, Y.; Bazant, Z.: Markov process model for random growth of crack with r-curve: Markov process model. *Engineering Fracture Mechanics*, 57, 6, (1997), 593–608.

Address: Universität Siegen, Fakultät IV, Dept. Maschinenbau, Lehrstuhl für Festkörpermechanik, Paul-Bonatz-Str. 9-11, D-57076 Siegen, Germany
email: `tim.korzeniowski | kerstin.weinberg@uni-siegen.de`